THE JOURNAL OF PHYSICAL CHEMISTRY A LETTERS

2009, *113,* 9261–9265
Published on Web 06/09/2009

Multiple Quantum Coherence Spectroscopy

Nathan A. Mathew, Lena A. Yurs, Stephen B. Block, Andrei V. Pakoulev, Kathryn M. Kornau, and John C. Wright*

Department of Chemistry, University of Wisconsin—Madison, Madison, Wisconsin 53706

Received: April 10, 2009; Revised Manuscript Received: May 22, 2009

Multiple quantum coherences provide a powerful approach for studies of complex systems because increasing the number of quantum states in a quantum mechanical superposition state increases the selectivity of a spectroscopic measurement. We show that frequency domain multiple quantum coherence multidimensional spectroscopy can create these superposition states using different frequency excitation pulses. The superposition state is created using two excitation frequencies to excite the symmetric and asymmetric stretch modes in a rhodium dicarbonyl chelate and the dynamic Stark effect to climb the vibrational ladders involving different overtone and combination band states. A monochromator resolves the free induction decay of different coherences comprising the superposition state. The three spectral dimensions provide the selectivity required to observe 19 different spectral features associated with fully coherent nonlinear processes involving up to 11 interactions with the excitation fields. The different features act as spectroscopic probes of the diagonal and off-diagonal parts of the molecular potential energy hypersurface. This approach can be considered as a coherent pump−probe spectroscopy where the pump is a series of excitation pulses that prepares a multiple quantum coherence and the probe is another series of pulses that creates the output coherence.

Introduction

Multiple quantum coherence (MQC) methods are a key tool for nuclear magnetic resonance's ability to obtain detailed structural information in proteins.[1] It is important to explore their potential as probes of electronic and vibrational states.[2] A MQC is a quantum mechanical superposition state formed by exciting a series of states on time scales that are short compared to the dephasing times of the MQC. Each pair of states (e.g., b and a) in the superposition represents a coherence that emits light at the difference frequency, ω_{ba}.[3] Each coherence is described by an off-diagonal density matrix element, $\rho_{ba} \equiv c_b c_a^*$, where c_a is the amplitude for state a in the MQC. A coherence emits light in beams whose directions are defined by the phase matching conditions of a nonlinear experiment. In order to achieve the widest range of applicability, it is important to have methods for creating MQCs containing states of diverse frequencies. In this paper, we demonstrate the feasibility of creating MQCs using frequency domain multiple quantum coherence multidimensional spectroscopy (MQC-MDS). Frequency domain MDS is particularly well-suited for creating MQCs because it only requires short-term phase coherence between the multiple excitation beams during the times they interact with a sample. The excitation beams can therefore have different frequencies and can excite any combination of quantum states.

In this paper, we demonstrate the feasibility of creating MQCs using frequency domain multiple quantum coherence multidimensional spectroscopy (MQC-MDS) involving up to eleven interactions with electromagnetic fields. The process uses the dynamic Stark effect[4−6] to climb vibrational ladders involving a series of coherences. The coherences are created by N-wave mixing where N is even and as high as 12. Multidimensional spectra are obtained by using two independently tunable excitation pulses that resolve the different mixing orders and a monochromator to spectrally resolve the super-radiant emission from the superposition state's coherences. The use of multiple dimensions separates and resolves the coherent pathways associated with the different multiple quantum coherences. Vibrational ladder climbing has been carried out by others using transient absorption and ultrafast high energy pulses to sequentially create populations in highly excited vibrational overtone states.[7−9] The experiments in this paper are fully coherent and do not involve population relaxation effects.

Theory

MQC-MDS measures the intensity resulting from the nonlinear polarization induced in the sample by the excitation electric fields. A Taylor series can describe the nonlinear relationship between the polarization and the excitation fields:

$$P = \chi^{(1)}E + \chi^{(3)}E^3 + \chi^{(5)}E^5 + \chi^{(7)}E^7 + ...$$

where the even terms are suppressed in isotropic samples and $\chi^{(N-1)}$ defines N-wave mixing.[10] The higher order terms become important at high intensities. The net electric field is given by the sum of the excitation fields,

$$E = E_1^o e^{i(k_1 z - \omega_1(t-\tau_1))} + E_2^o e^{i(k_2 z - \omega_2(t-\tau_2))} + E_{2'}^o e^{i(k_{2'} z - \omega_{2'}(t-\tau_{2'}))} + c.c$$

where the subscripts define the frequency of each excitation field. The polarization is coherent and creates output beams in directions defined by the phase matching conditions. The phase

* Corresponding author.

10.1021/jp903337s CCC: $40.75

matching used for this work is $\vec{k}_{out} = \vec{k}_1 - \vec{k}_2 + \vec{k}_{2'}$. An output field is created by the free induction decay that occurs after the last excitation pulse.

Although this phase matching condition normally defines four wave mixing, N-wave mixing occurs in the same direction and has the same output frequency if one considers adding $\mathbf{k}_n - \mathbf{k}_n$ pairs of interactions to the phase matching expression (for example, $\vec{k}_1 - \vec{k}_2 + \vec{k}_{2'} + \vec{k}_{2'} - \vec{k}_{2'} = \vec{k}_1 - \vec{k}_2 + \vec{k}_{2'}$). Thus, any excitation beam can interact an odd number of times with the sample and still meet the phase matching condition. The anharmonicity of successively higher vibrational states shifts the resonance frequency, so it becomes increasingly difficult for the excitation frequency to remain resonant with multiple transitions. However, the experiments are done at intensities where dynamic Stark effects are important so the transitions are sufficiently broadened to allow significant excitation of highly energetic vibrational states.

Quantum mechanically, Liouville pathways describe the evolution of the coherences in a nonlinear experiment. In our experiments, the time ordering of the three pulses corresponds to temporally overlapping beams 1 and 2′ and delaying beam 2 by τ_{21}. This time ordering corresponds to triply vibrationally enhanced (TRIVE) time orderings II and IV in previous work.[11,12] The fully resonant four wave mixing Liouville pathways are as follows:

$$gg \xrightarrow{1} bg \xrightarrow{2'} (a+b), g \xrightarrow{-2} bg \quad \text{and} \quad gg \xrightarrow{2'} ag \xrightarrow{1} (a+b), g \xrightarrow{-2} (a+b), a$$

respectively. The letters designate the ket- and bra- states (using Dirac notation) forming each coherence and the numbers represent the interacting fields that create each coherence.[10] Both pathways are fully coherent (they do not include intermediate populations) and include the double quantum coherence $(a+b),g$. The absence of populations has the advantage that population relaxation effects do not appear.[13] Population relaxation can create new peaks and cause the spectrum to evolve in time.

Although population relaxation does not complicate fully coherent pathways, coherence transfer can cause new peaks.[14−16] In coherence transfer, the thermal bath causes a state in a coherence to evolve to a different state without the loss of phase information. An example of coherence transfer is the Liouville pathway

$$gg \xrightarrow{1} bg \overset{CT}{\Rightarrow} ag \xrightarrow{2'} 2a, g \xrightarrow{-2} ag$$

where CT designates the coherence transfer step. This example requires two other equivalent time orderings that must be considered to fully describe coherence transfer.

Experimental Section

The experiment uses a mode-locked Ti:sapphire oscillator/regenerative amplifier to pump two optical parametric amplifiers (OPAs). Each OPA generates a tunable pulsed beam in the mid-infrared (ω_1 and ω_2), one of which is split to create the third pulse ($\omega_{2'}$). The pulse width is 900 fs and the bandwidth is ∼20 cm^{-1}. The beams, all vertically polarized, are focused into the sample by an off-axis parabolic mirror and aligned at angles which satisfy the FWM phase-matching condition, $\mathbf{k}_{out} = \mathbf{k}_1 - \mathbf{k}_2 + \mathbf{k}_{2'}$. A monochromator at ω_m and an HgCdTe detector measure the spatially isolated signal beam. The signal depends on five variables- the frequencies ω_1, ω_2, ω_m, and the time delays, τ_{21} and $\tau_{2'1}$ ($\tau_{ij} = \tau_i - \tau_j$, where τ_i defines the temporal position of the i^{th} excitation beam). Multidimensional spectra are obtained by scanning several variables with the others fixed. Two polarizers control the excitation intensities.

TABLE 1: Frequencies (in cm^{-1}) of the Asymmetric (Represented by *a*) and Symmetric (Represented by *b*) Stretch Overtone and Combination Band States Used in This Work

*a**b*	0	1	2	3	4	5	6
0	0	2084	4156	6218	8268	10306	12331
1	2015	4073	6123	8166			
2	4016	6047	8077				
3	6004						
4	7977						

The sample is a saturated hexane solution of rhodium(I) dicarbonyl acetylacetonate (RDC) in a 125 μm path length cell. The 2D-IR spectrum of RDC is well-known.[17] It consists of diagonal and cross peaks involving the asymmetric (mode a) and symmetric (mode b) modes with stretch frequencies of 2015 cm^{-1} and 2084 cm^{-1}, respectively. Each peak is oval and symmetrical as expected for homogeneously broadened transitions. The energies of the overtone and combination band states used in this work are summarized in Table 1. The values in Table 1 were determined from the work described in this letter and a series of higher-order wave mixing experiments that will be reported at a later time. There is very good agreement with results reported previously for the fundamentals, first overtones, and the combination band.[18,19]

Results and Discussion

Figure 1 shows the two-dimensional spectrum resulting from scanning ω_2 and ω_m over the range of the symmetric and asymmetric modes while maintaining $\omega_1 = 2078$ cm^{-1}, $\tau_{21} = 1.5$ ps, and $\tau_{2'1} = 0.00$ ps. The ω_1 value was selected because it was intermediate between the frequency of the $g \rightarrow b$ and the $b \rightarrow 2b$ transitions and could therefore improve the MQC excitation efficiency for higher vibrational states. The monochromator at ω_m isolates the free induction decay of the emitting coherence. Note that the monochromator's bandwidth is narrower than the excitation fields and consequently the spectral features are sharper along the ω_m axis. The frequency of the free induction decay defines the particular overtone or combination band transition. The optimal ω_2 frequency for a peak is not determined by a specific transition since ω_2 excites multiple transitions having different frequencies. The optimal ω_2 frequency reflects a compromise between the multiple transitions requiring excitation at ω_2.

At low excitation intensities, this spectrum has symmetrical peaks as observed in previous work.[17] However, when the excitation intensity is raised, the peaks develop the new asymmetrical structures that appear in figure 1. The excitation pulse intensities are $\sim 10^9$ watts/cm^2, so dynamic Stark effects and higher order wave mixing are important. The fully resonant four wave mixing peaks expected in the diagonal region of the spectrum are labeled 6 and 1, respectively. Similarly, the fully resonant four wave mixing peaks expected in the cross-peak region are labeled 14 and 16, respectively. However, many more peaks appear in the spectrum because of the higher order wave mixing. The assignments for the different labeled peaks are summarized in Table 2. Peak 5, although quite weak, appears reproducibly in spectra where the stronger features are saturated.

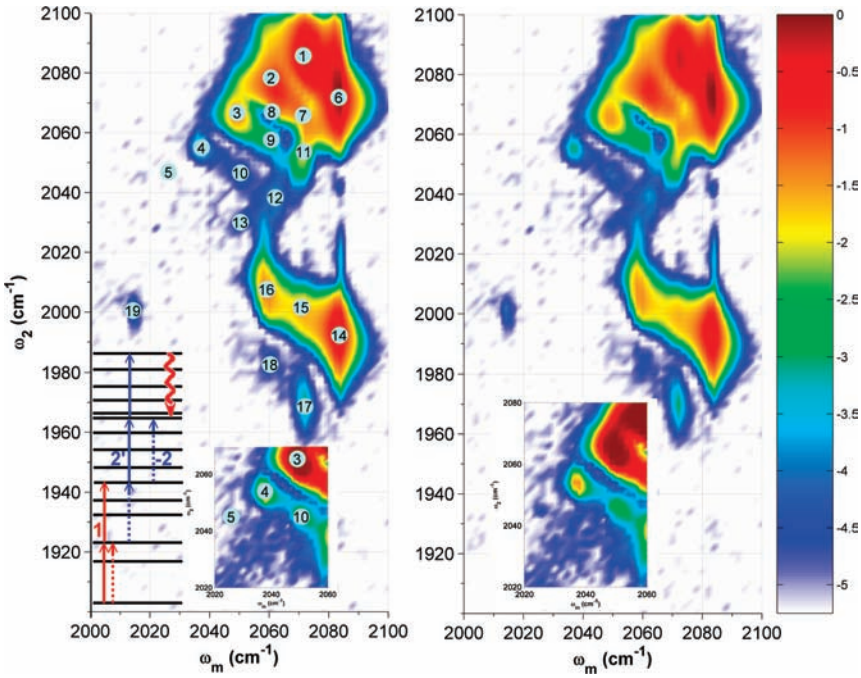

Figure 1. Two dimensional spectrum varying ω_2 and ω_m with $\omega_1 = 2078$ cm^{-1}, $\tau_{21} = 1.5$ ps, and $\tau_{2'1} = 0$ ps. The left side labels the spectral features and shows an example WMEL diagram for peak 3. The solid, dotted, and wavy arrows represent the ket state, the bra state, and the output state transitions, respectively. The inset shows the region of a reproducible feature labeled peak 5 obtained when the intensities of the more intense features are saturated. Peak 5 appears above the background with a signal-to-noise value of 7. The logarithmic scale spans 4 orders of magnitude.

An example appears as the inset where peak 5 is measurable above the background with a signal-to-noise of 7. The feature along the diagonal of this scan below peak 5 results from scatter from an excitation beam into the monochromator and is not four wave mixing signal. There are many equivalent Liouville pathways that create the same output coherence and each must be considered in quantitative models for MQC-MDS. The table shows only one representative pathway for each peak. The table also shows an estimate for the optimal ω_2 value for each peak assuming the optimal value is the average ω_2 frequency of all transitions involving ω_2.

In the region of the diagonal features, the peaks labeled 1−5 are the clearest sequence of $|v\rangle\langle v-1|$coherences involving successively higher values of vibrational quanta, v. As a specific example, a representative MQC pathway for peak 3 is

$$gg \xrightarrow{1} bg \xrightarrow{1} 2b, g \xrightarrow{-1} 2b, b \xrightarrow{2'} 3b, b \xrightarrow{2'} 4b, b \xrightarrow{-2'} 4b, 2b \xrightarrow{-2} 4b, 3b$$

Figure 1 contains a wave mixing energy level (WMEL) diagram[10] that illustrates the resonances in this pathway. The value of $\omega_1 = 2078$ cm^{-1} is midway between the values required for the $g \rightarrow b$ and $b \rightarrow 2b$ transitions while the value of $\omega_2 = 2062$ cm^{-1} is the average transition frequency of the $2b \rightarrow 3b$, $3b \rightarrow 4b$, $b \rightarrow 2b$, and $2b \rightarrow 3b$ transitions in this pathway. The monochromator frequency $\omega_m = 2050$ cm^{-1} matches that expected for the $|4b\rangle\langle 3b|$ coherence. Peak 3 requires 7 interactions to create the output coherence. The other peaks differ in the average number of interactions required to create the output coherence and the relative importance of the ω_1 and ω_2 excitation fields (see Table 2 for representative examples).

There are also spectral features lying below the $1 \rightarrow 5$ peak sequence. These peaks result when the coherent pathway involves intermediate multiple quantum coherences having vibrational quantum numbers that exceed those of the emitting coherence. The higher vibrational states have larger anharmonicities that require lower ω_2 frequencies for optimal excitation. For example, a representative pathway for peak 10 is

$$gg \xrightarrow{1} bg \xrightarrow{1} 2b, g \xrightarrow{-1} 2b, b \xrightarrow{1} 3b, b \xrightarrow{-1} 3b, 2b \xrightarrow{2'} 4b, 2b \xrightarrow{2'} 5b, 2b \xrightarrow{-2'} 5b, 3b \xrightarrow{-2} 4b, 3b$$

It has the same $4b$,$3b$ output coherence as peak 3 but it involves two additional interactions with the ω_2 field that create more energetic states with larger anharmonicities.

In the region of the cross-peak features, peaks 14 and 16 arise from the fully resonant four wave mixing pathways involving time orderings II and IV, respectively. Peak 15 arises from a six wave mixing pathway involving time ordering IV, but this pathway is optimized when ω_2 lies between the $g \rightarrow a$ and the $b \rightarrow a + b$ transitions. Peaks 17 and 18 also result from six wave mixing pathways involving MQCs. Peak 19 results from a coherence transfer pathway and it is discussed in previous publications.[14−16]

This paper uses a simplified and qualitative description of the MQC spectrum, but it is important to develop a quantitative model that properly accounts for the dynamic Stark effects, the excitation pulse bandwidth, and quantum mechanical interference effects. Nonperturbative theoretical approaches are well-suited to describing the experiment.[20] We will also report results on the excitation intensity dependence of the 2D spectrum in a forthcoming publication.

Conclusions

MQC-MDS has a number of important characteristics. The different MQCs probe diagonal and off-diagonal parts of the molecular potential energy hypersurface. It is therefore a valuable tool for measuring the shape of the potential energy

TABLE 2: Representative Coherence Pathways, Measured Value for the Output Coherence Frequency ω_m (in cm^{-1}), and the Predicted Average Value for ω_2 (in cm^{-1}) over the Different Interactions Involving ω_2 for the Different Features in Figure 1

peak	representative Liouville pathways	ω_m (cm^{-1})	ω_2 (cm^{-1})
1	$gg \xrightarrow{2'} bg \xrightarrow{1} 2b, g \xrightarrow{-2} 2b, b$	2072	2084
2	$gg \xrightarrow{2'} bg \xrightarrow{2'} 2b, g \xrightarrow{-2'} 2b, b \xrightarrow{1} 3b, b \xrightarrow{-2} 3b, 2b$	2062	2078
3	$gg \xrightarrow{1} bg \xrightarrow{1} 2b, g \xrightarrow{-1} 2b, b \xrightarrow{2'} 3b, b \xrightarrow{2'} 4b, b \xrightarrow{-2'} 4b, 2b \xrightarrow{-2} 4b, 3b$	2050	2061.5
4	$gg \xrightarrow{1} bg \xrightarrow{1} 2b, g \xrightarrow{-1} 2b, b \xrightarrow{2'} 3b, b \xrightarrow{-2'} 3b, 2b \xrightarrow{2'} 4b, 2b \xrightarrow{2} 5b, 2b \xrightarrow{-2} 5b, 3b \xrightarrow{-2} 5b, 4b$	2038	2055.7
5	$gg \xrightarrow{1} bg \xrightarrow{1} 2b, g \xrightarrow{-1} 2b, b \xrightarrow{1} 3b, b \xrightarrow{-1} 3b, 2b \xrightarrow{2'} 4b, 2b \xrightarrow{-2'} 4b, 3b \xrightarrow{2'} 5b, 3b \xrightarrow{2} 6b, 3b \xrightarrow{-2} 6b, 4b \xrightarrow{-2} 6b, 5b$	2025	2043.8
6	$gg \xrightarrow{1} bg \xrightarrow{2'} 2b, g \xrightarrow{-2} bg$	2084	2072
7	$gg \xrightarrow{1} bg \xrightarrow{1} 2b, g \xrightarrow{-1} 2b, b \xrightarrow{2'} 3b, b \xrightarrow{-2} 2b, b$	2072	2062
8	$gg \xrightarrow{1} bg \xrightarrow{1} 2b, g \xrightarrow{-1} 2b, b \xrightarrow{2'} 3b, b \xrightarrow{-2} 3b, 2b$	2062	2067
9	$gg \xrightarrow{1} bg \xrightarrow{1} 2b, g \xrightarrow{-1} 2b, b \xrightarrow{2'} 3b, b \xrightarrow{2'} 4b, b \xrightarrow{-2'} 4b, 2b \xrightarrow{-2} 3b, 2b$	2062	2058.5
10	$gg \xrightarrow{1} bg \xrightarrow{1} 2b, g \xrightarrow{-1} 2b, b \xrightarrow{1} 3b, b \xrightarrow{-1} 3b, 2b \xrightarrow{2'} 4b, 2b \xrightarrow{2'} 5b, 2b \xrightarrow{-2'} 5b, 3b \xrightarrow{-2} 4b, 3b$	2050	2047
11	$gg \xrightarrow{1} bg \xrightarrow{1} 2b, g \xrightarrow{-1} 2b, b \xrightarrow{1} 3b, b \xrightarrow{-1} 3b, 2b \xrightarrow{2'} 4b, 2b \xrightarrow{2'} 4b, b \xrightarrow{-2'} 3b, b \xrightarrow{-2} 2b, b$	2072	2058.5
12	$gg \xrightarrow{1} bg \xrightarrow{1} 2b, g \xrightarrow{-1} 2b, b \xrightarrow{1} 3b, b \xrightarrow{-1} 3b, 2b \xrightarrow{2'} 4b, 2b \xrightarrow{2'} 5b, 2b \xrightarrow{-2'} 4b, 2b \xrightarrow{2'} 5b, 2b \xrightarrow{-2'} 4b, 2b \xrightarrow{-2} 3b, 2b$	2062	2042
13	$gg \xrightarrow{1} bg \xrightarrow{1} 2b, g \xrightarrow{-1} 2b, b \xrightarrow{1} 3b, b \xrightarrow{-1} 3b, 2b \xrightarrow{1} 4b, 2b \xrightarrow{-1} 4b, 3b \xrightarrow{2'} 5b, 3b \xrightarrow{2'} 6b, 3b \xrightarrow{-2'} 5b, 3b \xrightarrow{-2} 4b, 3b$	2050	2032
14	$gg \xrightarrow{1} bg \xrightarrow{2'} (a + b), g \xrightarrow{-2} bg$	2084	1989
15	$gg \xrightarrow{2'} ag \xrightarrow{1} ab \xrightarrow{-1} (a + b), b \xrightarrow{1} (a + 2b), b \xrightarrow{-2} 2b, b$	2072	1991
16	$gg \xrightarrow{2'} ag \xrightarrow{1} (a + b), g \xrightarrow{-2} (a + b), a$	2058	2015
17	$gg \xrightarrow{1} bg \xrightarrow{1} 2b, g \xrightarrow{-1} 2b, b \xrightarrow{2'} (a + 2b), b \xrightarrow{-2} 2b, b$	2072	1967
18	$gg \xrightarrow{1} bg \xrightarrow{2'} (a + b), g \xrightarrow{2'} (2a + b), g \xrightarrow{-2'} (2a + b), a \xrightarrow{-2} (a + b), a$	2058	1988
19	$gg \xrightarrow{1} bg \xRightarrow{CT} ag \xrightarrow{2'} 2a, g \xrightarrow{-2} ag$	2015	2001

surface. MQCs can also reduce inhomogeneous broadening if the frequency shifts of the a and b states in a $|b\rangle\langle a|$ coherence induced by the broadening are correlated. Correlation in the inhomogeneous broadening will make the ω_{ba} frequency difference smaller than the individual ω_{ag} or ω_{bg} frequency shifts. Fully resonant pathways that create MQCs are not subject to the same population relaxation effects as partially coherent pathways so the spectra reflect the direct couplings between quantum states. Finally, the need for only short-term phase coherence in the excitation fields allows frequency domain MQC-MDS to use different excitation frequencies so the mixture of states in an MQC is defined only by the ability to create coherent excitation fields. Although this work used a model system with strong transition moments, these multiple quantum coherence experiments should be applicable to the wider range of interesting molecular systems since higher order processes are commonly encountered at high excitation intensities.

Acknowledgment. This work was supported by the National Science Foundation under Grant CHE-0650431.

References and Notes

(1) Mandal, P. K.; Majumdar, A. *Concepts Magn. Reson. Part A* **2004**, *20A*, 1.
(2) Pakoulev, A. V.; Rickard, M. A.; Meyers, K. A.; Kornau, K.; Mathew, N. A.; Thompson, D. C.; Wright, J. C. *J. Phys. Chem. A* **2006**, *110*, 3352.
(3) Scheurer, C.; Mukamel, S. *J. Chem. Phys.* **2002**, *116*, 6803.
(4) Ouellette, F.; Denariez-Roberge, M. M. *Can. J. Phys.* **1982**, *60*, 877.
(5) Winker, B. K.; Wright, J. C. *Opt. Lett.* **1989**, *14*, 54.
(6) Winker, B. K.; Wright, J. C. *Anal. Chem.* **1988**, *60*, 2599.
(7) Witte, T.; Yeston, J. S.; Motzkus, M.; Heilweil, E. J.; Kompa, K. L. *Chem. Phys. Lett.* **2004**, *392*, 156.
(8) Arrivo, S. M.; Dougherty, T. P.; Grubbs, W. T.; Heilweil, E. J. *Chem. Phys. Lett.* **1995**, *235*, 247.
(9) Kleiman, V. D.; Arrivo, S. M.; Melinger, J. S.; Heilweil, E. J. *Chem. Phys.* **1998**, *233*, 207.
(10) Wright, J. C. *Int. Rev. Phys. Chem.* **2002**, *21*, 185.
(11) Meyer, K. A.; Thompson, D. E.; Wright, J. C. *J. Phys. Chem. A* **2004**, *108*, 11485.
(12) Besemann, D. M.; Meyer, K. A.; Wright, J. C. *J. Phys. Chem. B* **2004**, *108*, 10493.
(13) Kurochkin, D. V.; Naraharisetty, S. R. G.; Rubtsov, I. V. *Proc. Natl. Acad. Sci. U.S.A.* **2007**, *104*, 14209.
(14) Pakoulev, A. V.; Rickard, M. A.; Mathew, N. A.; Kornau, K. M.; Wright, J. C. *J. Phys. Chem. A* **2008**, *112*, 6320.
(15) Rickard, M. A.; Pakoulev, A. V.; Mathew, N. A.; Kornau, K. M.; Wright, J. C. *J. Phys. Chem. A* **2007**, *111*, 1163.
(16) Pakoulev, A. V.; Rickard, M. A.; Mathew, N. A.; Kornau, K. M.; Wright, J. C. *J. Phys. Chem. A* **2007**, *111*, 6999.
(17) Golonzka, O.; Khalil, M.; Demirdoven, N.; Tokmakoff, A. *J. Chem. Phys.* **2001**, *115*, 10814.
(18) Khalil, M.; Demirdoven, N.; Tokmakoff, A. *J. Phys. Chem. A* **2003**, *107*, 5258.
(19) Khalil, M.; Demirdoven, N.; Tokmakoff, A. *J. Chem. Phys.* **2004**, *121*, 362.
(20) Mancal, T.; Pisliakov, A. V.; Fleming, G. R. *J. Chem. Phys.* **2006**, *124*, 234504.

JP903337S